Computer Methods and Programs in Biomedicine 142 (2017) 157–166

Contents lists available at ScienceDirect

Computer Methods and Programs in Biomedicine

journal homepage: www.elsevier.com/locate/cmpb

Vascular segmentation of head phase-contrast magnetic resonance angiograms using grayscale and shape features

Ruoxiu Xiao[a], Hui Ding[a], Fangwen Zhai[a], Tong Zhao[a], Wenjing Zhou[b], Guangzhi Wang[a,*]

[a] Department of Biomedical Engineering, School of Medicine, Tsinghua University, Room C249, Beijing 100084, China
[b] Tsinghua University Yuquan Hospital, No. 5, Shijingshan Road, Shijingshan District, Beijing, 100049, China

ARTICLE INFO

Article history:
Received 13 June 2016
Revised 24 January 2017
Accepted 9 February 2017

Keywords:
Neurosurgery
Vascular segmentation
Bayesian classification
Multiscale vascular enhancement
Dempster–Shafer evidence theory

ABSTRACT

Background and objective: In neurosurgery planning, vascular structures must be predetermined, which can guarantee the security of the operation carried out in the case of avoiding blood vessels. In this paper, an automatic algorithm of vascular segmentation, which combined the grayscale and shape features of the blood vessels, is proposed to extract 3D vascular structures from head phase-contrast magnetic resonance angiography dataset.

Methods: First, a cost function of mis-segmentation is introduced on the basis of traditional Bayesian statistical classification, and the blood vessel of weak grayscale that tended to be misclassified into background will be preserved. Second, enhanced vesselness image is obtained according to the shape-based multiscale vascular enhancement filter. Third, a new reconstructed vascular image is established according to the fusion of vascular grayscale and shape features using Dempster–Shafer evidence theory; subsequently, the corresponding segmentation structures are obtained. Finally, according to the noise distribution characteristic of the data, segmentation ratio coefficient, which increased linearly from top to bottom, is proposed to control the segmentation result, thereby preventing over-segmentation.

Results: Experiment results show that, through the proposed method, vascular structures can be detected not only when both grayscale and shape features are strong, but also when either of them is strong. Compared with traditional grayscale feature- and shape feature-based methods, it is better in the evaluation of testing in segmentation accuracy, and over-segmentation and under-segmentation ratios.

Conclusions: The proposed grayscale and shape features combined vascular segmentation is not only effective but also accurate. It may be used for diagnosis of vascular diseases and planning of neurosurgery.

1. Introduction

In the process of clinical diagnosis, the maximum intensity projection (MIP) [1] of computed tomography angiography (CTA) or magnetic resonance angiography (MRA) is often utilized for the diagnosis and treatment of vascular diseases. However, this technique cannot truly reflect the vascular structure in 3D space. Given that blood vessels and non-vascular tissues are present in angiograms, the segmentation of blood vessels from the dataset is the basis of quantitative diagnosis and treatment of vascular diseases [2,3]. Additionally, in the application of neurosurgery [4], specifically for the development of minimally invasive neurosurgery, such as electrode insertion for deep brain stimulation or locating the epileptogenic zone [5,6], how to guide surgical instruments to reach the planned area safely based on the preoperative imaging of blood vessels will also depend on the accurate segmentation of head vascular structures.

Currently, MRA is a commonly used vascular imaging modality in clinical settings. In addition to its high imaging resolution, patients do not need to receive radiation during angiography. According to whether contrast agent is injected or not, MRA can be divided into two kinds, namely contrast-enhanced MRA and noncontrast-enhanced MRA. In the former, contrast agent is injected into the patient's blood to obtain an enhanced angiographic image, and it is generally recognized as contrast-enhanced imaging. Certain studies have shown that some patients are prone to nephrogenic systemic fibrosis in the process of contrast agent injection; therefore, contrast enhancement MRA should be carefully conducted for clinical application. Noncontrast-enhanced MRA comprises time-of–flight (TOF), susceptibility-weighted imaging (SWI), and phase-contrast (PC) MRA. According to the angiography principle of TOF and SWI, these techniques mainly contain only a single imaging information of an artery or vein. Compared with TOF and SWI, PC-MRA is obtained according to the interaction

* Corresponding author.
E-mail address: wgz-dea@mail.tsinghua.edu.cn (G. Wang).

http://dx.doi.org/10.1016/j.cmpb.2017.02.008
0169-2607/

between blood flow and its gradient field; thus, non-vascular tissues will be suppressed, and both artery and vein structures are retained. Both structures of artery and vein should be considered in the procedures of clinical neurosurgery, so the extraction of vascular structure from the PC-MRA dataset is studied in this paper.

For the shape of blood vessels of head PC-MRA, the complexity of vascular network structures; variation in vascular direction, size, and curvature; and appearance of diseased vessels, specifically the geometry characterized caused by vasodilation, calcification, aneurysms, stenosis, and other diseases, are all factors that lead to the difficulty of vascular segmentation. For the grayscale of blood vessels of head PC-MRA, the intensity of small blood vessels appears low in images because of their slow flow rate, thereby making them difficult to be detected. Some noise is often detected in PC-MRA data, which is similar to the vessels in grayscale. Therefore, accurate and complete segmentation of the entire vascular network from the head PC-MRA data is a difficult task [7].

To date, most of the developed vascular segmentation algorithms can be divided into two types, namely grayscale- and shape-based methods. For grayscale-based methods, vascular structures are segmented from the dataset according to their grayscale distribution in angiograms; these methods include statistical model- [8–10], region growing- [11,12], active contour- [13], and level set-based [14] methods. Among them, statistical model-based methods are commonly utilized in the segmentation of blood vessels. These methods employ the Bayesian classification method, in which two or three grayscale functions are constructed to fit the image intensity distribution, and the vascular structures are subsequently extracted by optimizing the probability density function. For example, Wilson and Noble [15] introduced the Gaussian mixture model to describe the grayscale distributions of blood vessels and background; they used the expectation maximization (EM) algorithm to solve for the mixed probability density function and finally detected the vascular grayscale distribution area in angiograms. On this basis, Cauchy [16], Rician [17], double Sigmoid [18], Rayleigh [9], Gumbel [19], and many other distribution functions are also introduced to improve the statistical distribution function or optimization method [8]. However, the signal of small blood vessels is very weak, so they are inevitably lost because of truncation error in segmentation via the statistical model. Therefore, many researchers have considered adding other constraints based on the statistical model to complete the missing information. For example, Chung et al. [10,20] proposed a cerebral vascular segmentation method based on the statistical model and local phase coherence, which does not only extract normal large blood vessels but also recognizes the low grayscale area of aneurysm and vein. Hassouna et al. [9] introduced the Markov random field (MRF) in the application of a statistical model, and they also used the maximum pseudo likelihood estimation to optimize the parameters of 3D MRF; thus, the small size of the vascular structures is not destroyed. However, the above models are established in the situation that only a small amount of low-contrast vessels is present. If an image contains a considerable amount of noise, which is similar to the blood vessel in grayscale distribution, then vascular structures will be difficult to obtain by only using grayscale features.

The shape-based methods extract vascular structures in images through preconstructed models, which are achieved according to the tubular geometry of the vascular shape. Among them, tracking- and Hessian matrix-based methods are commonly studied. In tracking-based methods, some tubular structures are utilized as templates, and the important parameters of vascular centerline, diameter, and bifurcation are fit in the tracking procedure. For example, Friman et al. [21] modeled the centerline, direction, and sectional grayscale distribution in the tracking of local 3D vascular segment, and they fit the best matching degree of vascular segments to obtain the global vascular structures. Zhou et al. [22] used a Gabor filter to track the vascular segment of target structures, and the phase and amplitude of the Gabor filter were adjusted to fit the orientation and size of the local vascular segment. The tracking-based vascular segmentation methods are dependent on the setting of initial tracking points and end points; therefore, they are highly suitable for handling a small amount of vascular branches but not for the extraction of the entire 3D vascular network in head. The vascular grayscale turns from bright to dark when moving from the center to the edge because of the specific tubular structure of blood vessels, that is, the grayscale distribution of blood vessels exhibit a ridge characteristic. When reflected to the differential information of image, grayscale can be expressed by the Hessian matrix's eigenvalues, that is, the absolute of the Hessian matrix's eigenvalue is nearly equal to 0 in the direction of vascular centerline, but it is far larger than 0 in the directions perpendicular to the vascular centerline. According to this specific distribution of Hessian matrix's eigenvalues, the amount of vascular enhancement filters has been constructed through the combination of Hessian matrix's eigenvalues. To enhance all scales of vessels and protect the small blood vessels, a multiscale space is often constructed, and the vascular enhancement filters are performed by finding the optimized response in the multiscale space. Commonly used multiscale vascular enhancement filters have been proposed by Lorenz et al. [23], Sato et al. [24], and Frangi et al. [25]. In our previous work [26], we segmented the vascular structures of the brain region based on the multiscale vascular enhancement filter proposed by Frangi et al. Nevertheless, to construct a multiscale space, Gaussian functions of different standard deviations should be convoluted with angiograms. This measure causes the expansion of the vascular area in the image and results in over-segmentation.

In this paper, we propose an automatic vascular segmentation method via a combination of vascular grayscale and shape features; this method can accurately extract 3D vascular structures from the head PC-MRA dataset. First, according to the vascular grayscale distribution, the initial vascular segmentation is achieved through the improved Bayesian statistical model. Subsequently, the corresponding vesselness image of the original PC-MRA dataset is produced by applying a Hessian matrix-based multiscale enhancement filter. Based on the obtained initial vascular segmentation and enhanced vascular response image, the reconstructed vascular image is designed by combining with vascular grayscale and shape features, and a new vascular profile is segmented from it. To remove the interference of noise in the head PC-MRA dataset, we propose the segmentation ratio coefficient (SRC). According to the distribution of noise in angiograms, the SRC varies linearly from the top to bottom of the head PC-MRA dataset. The SRC can quantitatively control the final segmentation by removing noise in each slice.

2. Methods

To segment the entire vascular network from the head PC-MRA, we obtain the initial vascular contour according to the vascular grayscale feature. The vesselness image according to the vascular shape feature is then captured. The contour and vesselness image are combined according to the Dempster–Shafer evidence theory to construct the vascular reconstruction image, from which we extract the final vascular structure.

2.1. Initial segmentation based on grayscale feature

As illustrated in Fig. 1, PC-MRA image contains the background and vascular areas of low and high intensities, respectively; thus, the background and blood vessels can be distinguished based on

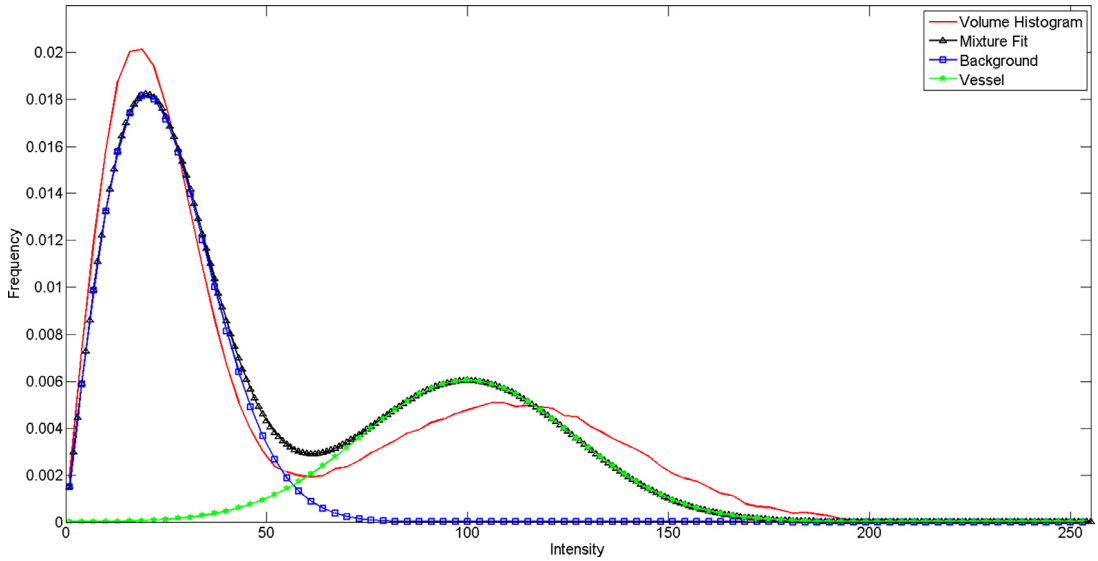

Fig. 1. Vascular segmentation model based on Bayesian classification. The curve with none is the histogram of the image, the curve with triangle is the estimated grayscale probability density distribution of the image, the curve with square is the grayscale probability density distribution function of the background, and the curve with pentagon is the grayscale probability density distribution function of blood vessel. Ω_1 is the feature space where the blood vessel is missegmented as background, and Ω_2 is the feature space where background is missegmented as the blood vessel.

these characters. In this process, according to Bayesian decision theory, we estimate the grayscale distribution function of the image by prior probability and class conditional density functions of background and blood vessels, assign different weights to calculate the mis-segmentation of background and blood vessels, minimize the risk of vascular missegmentation, and obtain the optimal parameters using the EM algorithm.

Let ω_1 and ω_2 be denoted as the background and blood vessel in the image, respectively. The grayscale distribution of image $p(x)$ can be expressed as follows:

$$p(X) = p(X|\omega_1)\mathrm{P}(\omega_1) + p(X|\omega_2)\mathrm{P}(\omega_2) \tag{1}$$

where, $p(X|\omega_1)$ is the conditional probability density function in which voxel X belongs to ω_1, and $p(X|\omega_2)$ is the conditional probability density function in which voxel X belongs to ω_2. $\mathrm{P}(\omega_1)$ is the priori probability of background, and $\mathrm{P}(\omega_2)$ is the priori probability of blood vessel.

In the procedure of vascular segmentation based on traditional Bayesian decision theory, the posterior probability density function $p(\omega_1|X)$ and $p(\omega_2|X)$ are utilized for the classification of background and blood vessel. If X satisfies the condition:

$$p(\omega_1|X) < p(\omega_2|X) \tag{2}$$

then X belongs to the blood vessel; otherwise, X belongs to the background. According to the Bayesian formula, Eq. (2) can be changed as follows:

$$p(\mathrm{X}|\omega_1)\mathrm{P}(\omega_1) < p(\mathrm{X}|\omega_2)\mathrm{P}(\omega_2) \tag{3}$$

Therefore, when $p(X|\omega_1)$, $p(X|\omega_2)$, $\mathrm{P}(\omega_1)$, and $\mathrm{P}(\omega_2)$ are available, voxel X can be determined as ω_1 or ω_2 through Eq. (3).

The grayscale distributions of background and blood vessel have a cross. When using Bayesian classification theory to segment the background and blood vessel, they are misclassified into the area of the background because of the presence of some small parts of blood vessels with low intensity (Fig. 1). Similarly, some parts of the background with high intensity are present and misclassified into the area of the blood vessel. However, the cost of misclassification in both cases is considered the same when using Eq. (3). Given that we can remove the noise in the post-processing stage, we hope to obtain more information about the blood vessels in the case of tolerating some noise, rather than try to classify background and blood vessel under the condition prior to filtering out noise. Therefore, we will differentiate the cost of these two misclassifications and use different weights to punish them. To quantify the risk of misclassification, we define the cost function as follows:

$$r = r_1 + r_2 := \lambda_1 P(\omega_1) \int_{\Omega_2} p(\mathrm{X}|\omega_1) + \lambda_2 P(\omega_2) \int_{\Omega_1} p(X|\omega_2) \tag{4}$$

where r_1 is the cost of X misclassified to ω_2, which belongs to ω_1, and λ_1 is its corresponding penalty coefficient. r_2 is the cost of X misclassified to ω_1, which belongs to ω_2, and λ_2 is its corresponding penalty coefficient. Ω_1 and Ω_2 are feature spaces of ω_1 and ω_2, respectively. In this paper, we define two penalty coefficients to satisfy the complementary condition, that is, $\lambda_1 + \lambda_2 = 1$. Therefore, if the penalty coefficient λ is defined as the penalty coefficient λ_2 corresponding to where blood vessel is misclassified into background, then Eq. (4) can be converted as follows:

$$r = (1-\lambda) P(\omega_1) \int_{\Omega_2} p(\mathrm{X}|\omega_1) + \lambda P(\omega_2) \int_{\Omega_1} p(X|\omega_2) \tag{5}$$

According to the above definition, the discriminant function (3) can be modified as follows:

$$\lambda p(\mathrm{X}|\omega_1)\mathrm{P}(\omega_1) < (1-\lambda) p(\mathrm{X}|\omega_2)\mathrm{P}(\omega_2) \tag{6}$$

Similar to the literature [9], to fit the histogram of each slice of PC-MRA, we use Rayleigh and Gaussian distributions to describe the background and blood vessel, respectively. Subsequently, $p(X|\omega_1)$ and $p(X|\omega_2)$ can be expressed as follows:

$$p(\mathrm{X}|\omega_1) = p(X, \sigma_1) = \frac{X}{\sigma_1} \exp\left[-\frac{X^2}{2\sigma_1^2}\right] \tag{7}$$

$$p(X|\omega_2) = p(X, \mu_2, \sigma_2) = \frac{1}{\sqrt{2\pi}\sigma_2} \exp\left[-\frac{(X-\mu_2)^2}{2\sigma_2^2}\right] \tag{8}$$

where σ_1 is the standard deviation of Rayleigh distribution, and μ_2 and σ_2 are the mean and standard deviation of Gaussian distribution, respectively.

To date, we have constructed the improved Bayesian classification through Eqs. (6)–(8). To obtain the corresponding optimized parameters, the EM algorithm is employed to estimate $p(X|\omega_1)$, $p(X|\omega_2)$, $\mathrm{P}(\omega_1)$, and $\mathrm{P}(\omega_2)$. The estimated results are substituted

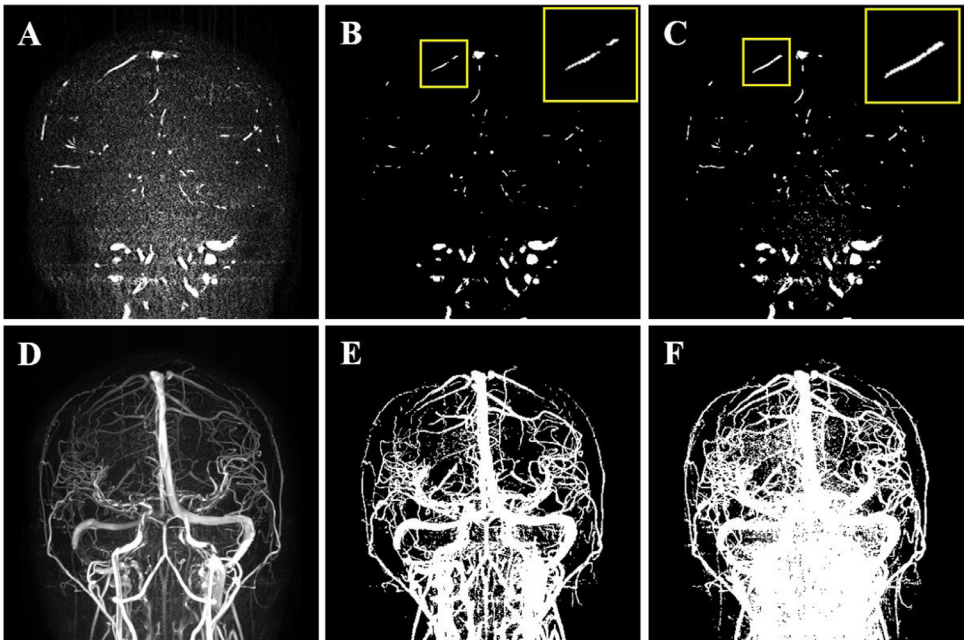

Fig. 2. Vascular segmentation results using Bayesian classification methods. (A) A slice of phase-contrast magnetic resonance angiography (PC-MRA). (B) Vascular segmentation result of (A) based on the traditional Bayesian classification method. (C) Vascular segmentation result of (A) based on the proposed improved Bayesian classification method. (D) Maximum intensity projection (MIP) image of the original 3D PC-MRA dataset. (E) MIP of 3D segmented vascular structures based on the traditional Bayesian classification method. (F) MIP of 3D segmented vascular structures based on the proposed improved Bayesian classification method.

into Eq. (6), and the initial vascular segmentation can be obtained based on grayscale feature.

As shown in Fig. 2, Fig. 2A is a slice of the PC-MRA dataset in the coronal direction, Fig. 2B is the segmentation result based on traditional Bayesian classification method, and Fig. 2C is the segmentation result based on the proposed improved Bayesian classification method (λ=0.99). Fig. 2E and F are the corresponding MIP results of the original data and vascular structures obtained through traditional Bayesian and proposed Bayesian methods. In order to enhance some key information of images, the same regions of Fig. 2B and C are enlarged, and it can been seen from the figures that, some vascular structures that cannot be detected in traditional methods can now be observed in our proposed method. Although a large amount of noise is also included in the segmentation result, it can be removed in the later process.

2.2. Vascular enhancement based on shape feature

According to the specific geometry of the blood vessel, we can also detect the vascular structure in the PC-MRA dataset. In this process, we use a multiscale Hessian matrix-based filter to enhance the vascular region and suppress the non-tubular region in the image, and finally obtain a normalized enhanced vesselness image.

Let H be denoted as the Hessian matrix of voxel $X(x, y, z)$, and it is defined as follows:

$$H(x,y,z) = \begin{pmatrix} \frac{\partial^2 I}{\partial x^2} & \frac{\partial^2 I}{\partial xy} & \frac{\partial^2 I}{\partial xz} \\ \frac{\partial^2 I}{\partial yx} & \frac{\partial^2 I}{\partial y^2} & \frac{\partial^2 I}{\partial yz} \\ \frac{\partial^2 I}{\partial zx} & \frac{\partial^2 I}{\partial zy} & \frac{\partial^2 I}{\partial z^2} \end{pmatrix} \tag{9}$$

H is the second-order partial derivative of voxel $X(x, y, z)$ in the directions of x, y and z, and the corresponding eigenvalues and eigenvectors of H can be expressed as λ_1, λ_2, λ_3 ($|\lambda_1| < |\lambda_2| < |\lambda_3|$) and v_1, v_2, v_3, respectively. In calculating the Hessian matrix, the image is supposed to be twice continuously differentiable; therefore, $\frac{\partial^2 I}{\partial xy}=\frac{\partial^2 I}{\partial yx}$, $\frac{\partial^2 I}{\partial xz}=\frac{\partial^2 I}{\partial zx}$, and $\frac{\partial^2 I}{\partial yz}=\frac{\partial^2 I}{\partial zy}$, that is, H is a symmetric matrix. According to the characteristics of a symmetric matrix, the eigenvectors are mutually orthogonal, that is, $v_1 \perp v_2 \perp v_3$.

When images are analyzed based on the Hessian matrix, their different eigenvalues and eigenvectors have different meanings [27]. For a 3D image, the maximum amplitude eigenvalue corresponds to the maximum curvature direction of voxel X, and the minimum amplitude eigenvalue corresponds to the minimum curvature direction of voxel X. Therefore, different shapes correspond to the different distributions of the Hessian matrix's eigenvalues. For tubular structures, the intensity of the vascular direction changes slowly, that is, $|\lambda_1| \approx 0$. By contrast, in the direction perpendicular to the blood vessel, the intensity changes severely, that is $|\lambda_2|, |\lambda_3| \gg 0$. The absolute symbol of eigenvalues can be removed depending on whether the structure is bright or dark in the image.

According to this characteristic, the Hessian matrix's eigenvalue-based filter can be constructed to enhance the tubular structure [23–25]. Although the enhancement forms of filter expression are not the same, the obtained results might be very similar [28]. In this paper, we use the vascular enhancement filter proposed by the literature [25] to obtain the vesselness image, and the corresponding enhancement expression is given as follows:

$$f(X,\sigma) = \begin{cases} 0, & \max(\lambda_2,\lambda_3) > 0 \\ \left[1-\exp\left(-\frac{\lambda_1^2}{2\alpha^2\lambda_3^2}\right)\right]\exp\left(-\frac{\lambda_1^2}{2\beta^2\lambda_2\lambda_3}\right) & \\ \quad \times\left[1-\exp\left(-\frac{\lambda_1^2+\lambda_2^2+\lambda_3^2}{2\gamma^2}\right)\right], & else \end{cases} \tag{10}$$

where α, β, and γ are enhancement parameters of the filer, and σ is the corresponding enhancement scale.

In the head PC-MRA dataset, blood vessels have a large difference of scales. For example, the sinus is large, whereas the vascular branches of multistage are small. Enhancement based on a single scale will be unreasonable because large-scale vessels cannot be detected through insufficient enhancement, and small vessels might be lost via excessive enhancement. Multiscale

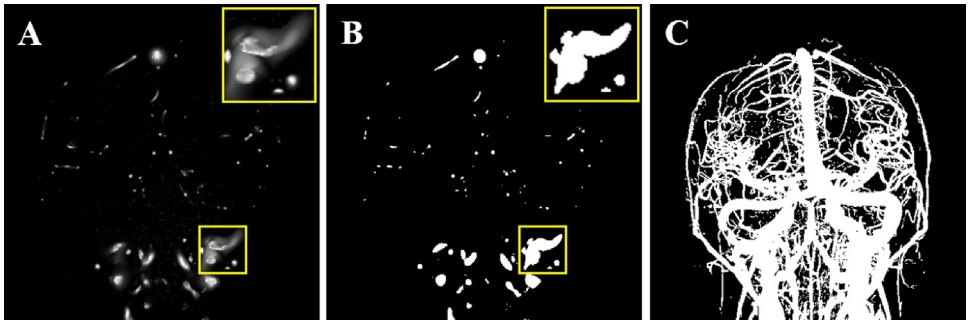

Fig. 3. Processing results of multiscale vascular enhancement. (A) Enhanced vesselness image of Fig. 2A; (B) Otsu vascular segmentation result of (A); and (C) coronal MIP result of the segmented 3D vascular structures based on the combination of the multiscale filter and Otsu method.

enhancement should be constructed to enhance and detect the vascular structures in the image. The construction of a multiscale space has a very important role in object detection in the image [29,30]. Objects can be identified, which are unrecognizable in a single scale space, through changing of scales. Thus, the multiscale-based enhancement filter will obtain a better enhanced result than a single scale-based enhancement filter. In this paper, through the predefinition of the sampling scale space $[\sigma_{\min}, \sigma_{\max}]$, the multiscale vascular enhancement filter result is determined as the voxel's highest enhanced response in the constructed multiscale space as follows:

$$f(X) = \max_{\sigma_{\min} \le \sigma \le \sigma_{\max}} f(X, \sigma) \tag{11}$$

Fig. 3A is the enhanced vesselness image of Fig. 2A, where scale is sampled in the range of [0.5, 10], Fig. 3B is the thresholding segmentation result of the Fig. 3A by Otsu algorithm [31], and Fig. 3C is the coronal MIP result of 3D vascular structures segmented based on the combined multiscale filter and Otsu method. The same regions of Fig. 3B and C are enlarged to enhance some key information of images, and it can been seen from the figures that, although a large number of blood vessels can be detected based on multiscale vascular enhancement, some vascular regions of vesselness image are expanded, which leads to segmented vessels become larger.

2.3. Vascular segmentation combined with grayscale and shape features

In this paper, a vascular image is reconstructed by vascular grayscale and shape features according to the Dempster–Shafer evidence theory [32], and then vascular structures are segmented from reconstruction image. It can sufficiently suppress noise according to its non-tubular structure and preserve small vessels after enhancement. Both features are utilized for the construction of the vascular reconstruction image, and the definition of SRC is then proposed, which linearly increases from the top to bottom of the head PC-MRA dataset. The segmentation result is compared with the initial segmentation structures, and the SRC is used to control over-segmentation.

According to the two sources Dempster–Shafer evidence theory, if two kinds of belief functions are denotes as $m_1(X)$ and $m_2(X)$, then the fused belief function $m(X)$ can be expressed as follows:

$$m(X) = \frac{1}{\mathrm{K}} m_1(X) m_2(X) \tag{12}$$

where, the normalization constant K is obtained as follows:

$$\mathrm{K} = m_1(X) m_2(X) + [1 - m_1(X)][1 - m_2(X)] \tag{13}$$

Let $G(X)$ be denoted as the vascular membership function constructed by vascular grayscale feature, and $S(X)$ be denoted as the vascular membership function constructed by vascular shape feature, then the vascular reconstruction image can be obtained when $m_1(X)=G(X)$ and $m_2(X)= S(X)$ are substituted into Eqs. (12) and (13).

The definition of $S(X)$ is achieved as the vesselness image according to the vascular shape feature, and $G(X)$ is defined as follows:

$$G(X) = \begin{cases} 0, & X < Thr_g \\ I(X), & else \end{cases} \tag{14}$$

where, Thr_g is the grayscale threshold determined by Eq. (6), and $I(X)$ is intensity value at voxel X.

In this paper, we combined the vascular grayscale and shape features by non-linear fusion. In the vascular reconstruction image, segmentation results of both features are retained, and the crossover region of these two features is highlighted. Therefore, we can segment the vascular structure not only where the grayscale feature or shape feature is strong, but also where the grayscale feature is weak but the shape feature is strong or where the shape feature is weak but the grayscale is strong.

Based on the obtained vascular reconstruction image, we use the Otsu method to segment it and then obtain the corresponding segmentation result V. The definition of SRC T_i is proposed to verify the segmentation result in each slice by comparing with the initial segmentation A and V, and it can control over-segmentation while retaining the real vascular structures as much as possible. The operation is given as follows:

$$V_i^* = \begin{cases} V_i, & if \ \frac{A_i}{V_i} > T_i \\ A_i, & else \end{cases} \tag{15}$$

where T_i is denoted as the SRC corresponding to slice i, V_i is the reconstructed result of V in slice i, A_i is the segmentation result of A in slice i, and V_i^* is expressed as the newly reconstructed result controlled by SRC T_i in slice i.

In the process of PC-MRA imaging, more vessels exist in the neck than in the top of the head, and flow is faster in the neck than in the top of head, which leads to more noise in the image. Therefore, more noise is present in the bottom of the dataset than in the top. According to this characteristic, SRC is designed as linearly increasing from the top T_{top} to the bottom T_{bottom}, and a more accurate vascular segmentation result will be obtained. In practice, the top of SRC T_{top} is defined as 1, whereas the bottom is defined as $T_{\max}$; hence, the range of SRC is [1, $T_{\max}$].

Fig. 4 provides the vascular segmentation results based on the proposed method. Fig. 4A shows the result based on the proposed method in a slice. Fig. 4B is the coronal MIP of the 3D segmentation vascular structures, Fig. 4C is the denoising result of Fig. 4B obtained through the proposed SRC, and Fig. 4D is the corresponding removed noise. Compared with the grayscale feature-based segmentation, the proposed method can not only

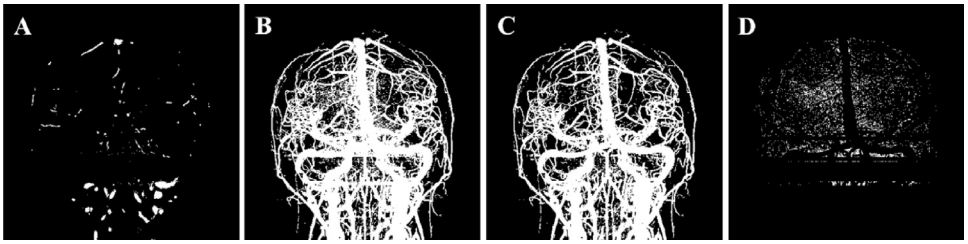

Fig. 4. Vascular segmentation results of our proposed method. (A) Vascular structures segmented in a slice; (B) MIP of the segmented 3D vascular structures; (C) corresponding denoising result of (B); and (D) removed noise of (B).

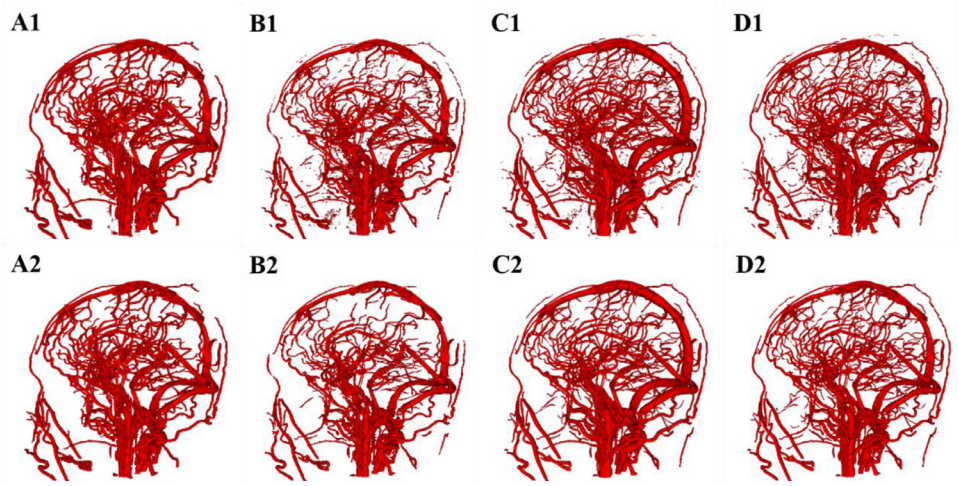

Fig. 5. 3D rendering of different vascular segmentation results. (A1) Manual vascular segmentation result; (B1) Grayscale-based vascular segmentation result; (C1) shape-based vascular segmentation result; and (D1) proposed vascular segmentation result. (A2)–(D2) Corresponding denoising results of (A1)–(D1), respectively.

obtain the structures that can be extracted via the traditional Bayesian classification method but also reduce the noise brought in the procedure by our proposed improved Bayesian classification. Compared with the shape feature-based segmentation, the proposed method also removes over-segmentation and retains the actual vascular structures.

3. Experimental results

To evaluate the feasibility and effectiveness of the proposed algorithm, data from 10 epilepsy patients without any cerebral vascular diseases provided by Tsinghua University Imaging Center, which are collected from July 2015 to September 2015, and tested in this paper. All patients were prospectively recruited under the approval from Institutional Review Board, and informed consent was obtained from all subjects for being included in the study. The clinical dataset comprises four men and six women, with ages between 9 and 46 years old (average age = 26.2 years). The PCA-MRA datasets are evaluated on a 3T Philips Medical MRI Systems (Achieva) using a 32-channel head coil. The main angiography parameters are as follows: repetition time = 10 ms, echo time = 10 ms, flip angle = 15°, SENSE = 6, velocity encoding value = 20 cm/s, resolution of obtained PC-MRA dataset = $400 \times 400 \times 330$, and voxel size = 0.5 mm × 0.5 mm × 0.6 mm.

First, the feasibility of the proposed algorithm is evaluated through visualizing the segmented vascular structure. Fig. 5A1, B1, C1 and D1 correspond to the vascular reconstruction result of the manual segmentation, grayscale-based method proposed by Chung [10], shape-based method proposed by Du [26], and proposed grayscale and shape combined method, respectively. Fig. 5A2, B2, C2 and D2 are the denoising results of Fig. 5A1, B1, C1 and D1 through the connected filter, respectively. To display the vascular structure intuitively, the marching cube (MC) algorithm [33] is used for rendering, and a realistic vascular surface reconstruction can be obtained. When applying the grayscale-based method, small vessels might be lost during structure reconstruction because many small vessels of low intensity are present in the dataset. When applying the shape-based method, over-segmentation is present, specifically for the venous sinus, because vessels are enlarged during convolution with Gaussian functions. Using our proposed segmentation, the vascular grayscale and shape features are combined, complete information of vascular structure can be retained, and over-segmentation is avoided.

In experiments, algorithms are implemented in Microsoft Visual Studio 2010 on an Intel Core i7 PC (with CPU 3.5 G and 16 G memory). The average of computational time for grayscale-based method, shape based-method and proposed method are 30 minutes, 5 minutes and 35 minutes, respectively.

To reflect the segmentation of vascular structures and corresponding original dataset accurately, the segmented 3D vascular structures are projected onto the 2D planes through the MIP algorithm to compare with the MIP of the original PC-MRA dataset.

Fig. 6A1, B1, C1 and D1 give the MIP results of original data and segmented results of the grayscale-based method, shape based-method, and proposed method, respectively, in the direction of sagittal. In order to clear observe the comparison between them, two typical areas are enlarged and displayed in the second and third rows of Fig. 6. In comparison with the original image, it can be seen that, if vascular structures are segmented just based their grayscale feature, some regions of weak grayscale would be lost (Fig. 6B2). For our proposed algorithm, vascular shape feature is combined to extract this weak information, and they can be detected in Fig. 6D2. In the process of multiscale enhancing, multiscale space is constructed via convolution with Gaussian functions, so the edge of the blood vessels will be blurred, specifically for the large vessels, thereby leading to over-segmentation. Therefore,

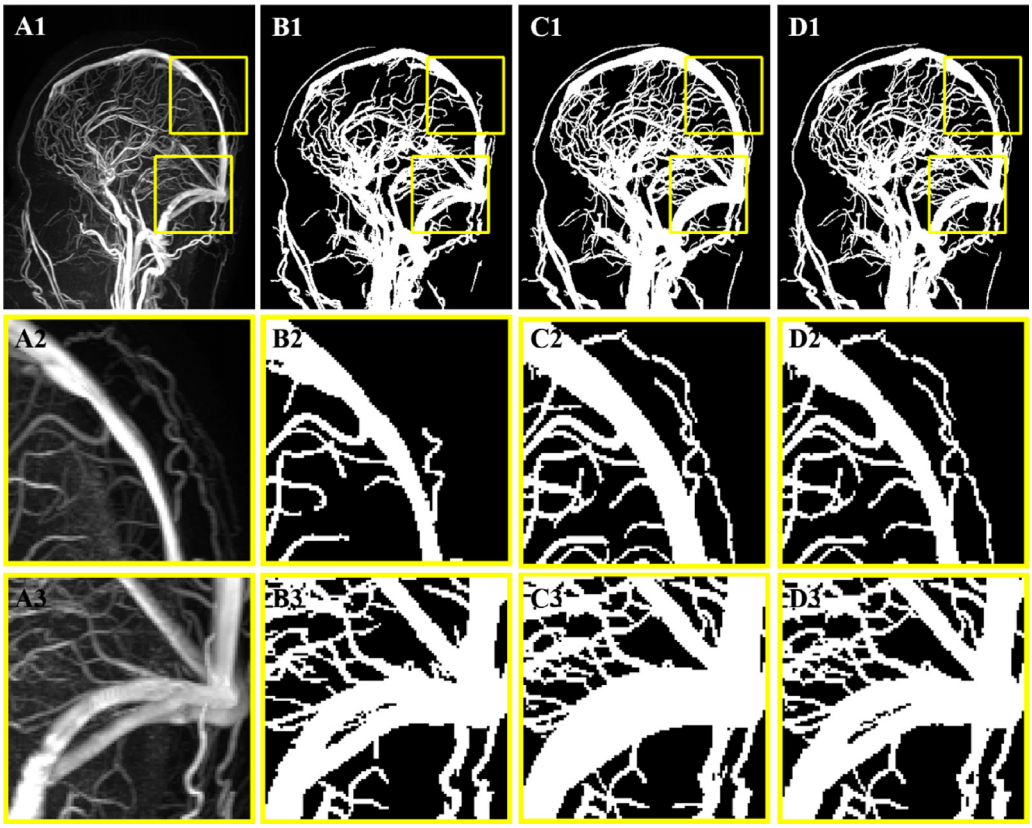

Fig. 6. MIP of the PC-MRA dataset and segmented 3D vascular structures. (A1) Original dataset; (B1) Grayscale-based vascular segmentation result; (C1) shape-based vascular segmentation result; and (D1) proposed vascular segmentation result. (A2)–(D2) and (A3)-(D3) are corresponding enlarged results of (A1)–(D1), respectively.

if segment vascular structures only based on their shape feature, over-segmentation would be caused in some regions (Fig. 6C2 and C3). In our method, we use their grayscale feature to limit it. And it can be seen from Fig. 6D2 and D3, the over-segmentation is well controlled. From visualization of the comparison, with our proposed segmentation method, the entire vascular structures can be extracted, and they are consistent with the actual structures.

To validate these observations, we analyzed the proposed algorithm by considering the manual segmentation of the PC-MRA dataset as ground truth. The dice similarity coefficient (DSC), false positive rate (FPR), and false negative rate (FNR) are used to express the measurement of the segmentation, over-segmentation, and under-segmentation ratios, respectively. According to the literature [19], the definitions of DSC, FPR, and FNR are as follows:

$$DSC = \frac{2 \times (AS \cap GT)}{AS + GT} \tag{16}$$

$$FPR = \frac{AS \cap GT^c}{GT} \tag{17}$$

$$FNR = \frac{AS^c \cap GT}{GT} \tag{18}$$

where AS is the result of automatic segmentation, and GT is the result of manual segmentation.

To obtain the most effective performance of segmentation, we evaluate the penalty coefficient in the procedure of the improved Bayesian classification (λ in Eq. (6)). Fig. 7 provides the relationship between DSC, FPR, FNR, and the changes in the penalty coefficient when the penalty coefficient is sampled in [0.05, 0.99] with the sampling interval of 0.05. When the penalty coefficient increases from 0.05 to 0.95 and 0.95 to 0.99, the DSC of the proposed algorithm initially increases from 0.731 to the maximum of 0.834 and decreases to 0.799; the FPR decreases slowly from 0.407 to 0.155 and immediately decreases to 0.029; the FNR increases slowly from 0.029 to 0.181 and then increases to 0.461. Therefore, when the penalty coefficient is 0.95, the DSC is optimal. Although FPR and FRP are not the most effective, they are acceptable. Hence, 0.95 can be determined as the optimal choice of the penalty coefficient.

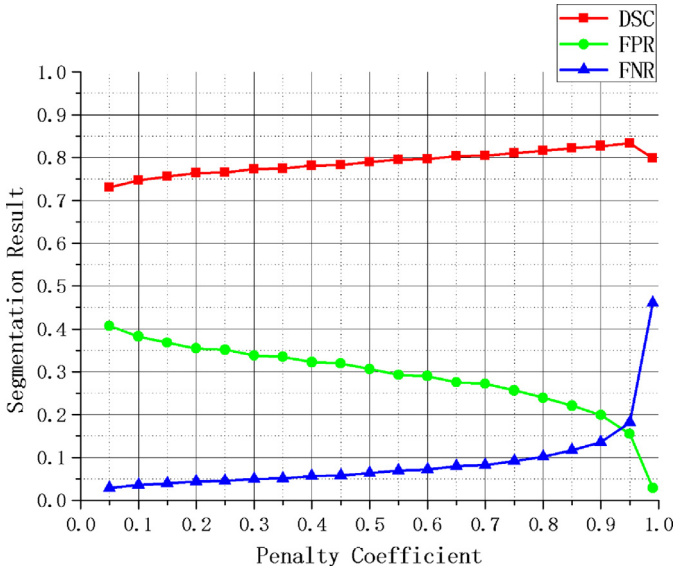

Fig. 7. Relationship between dice similarity coefficient (DSC), false positive rate (FPR), and false negative rate (FNR) and the changes in the penalty coefficient.

Table 1
Comparison of the segmentation results of the grayscale-based method, shape-based method, and proposed method for 10 head PC-MRA datasets.

	Sex	Age	Grayscale based method [10]			Shape based method [26]			Proposed method		
			DSC	FPR	FNR	DSC	FPR	FNR	DSC	FPR	FNR
Data1	M	20	0.790	0.063	0.306	0.702	0.428	0.227	0.839	0.208	0.095
Data2	F	27	0.808	0.046	0.219	0.708	0.500	0.178	0.802	0.224	0.181
Data3	M	14	0.734	0.079	0.386	0.679	0.730	0.110	0.822	0.277	0.109
Data4	F	34	0.859	0.077	0.209	0.674	0.771	0.100	0.832	0.262	0.101
Data5	F	25	0.604	**1.290**	0.009	0.729	0.336	0.234	0.778	0.202	0.235
Data6	M	37	0.788	0.507	0.021	0.644	**0.926**	0.085	0.803	0.364	0.086
Data7	F	46	0.766	0.086	0.318	0.718	0.554	0.130	0.832	0.221	0.129
Data8	M	24	0.553	**1.610**	0.002	0.704	0.596	0.134	0.766	0.394	0.134
Data9	F	9	0.849	0.331	0.018	0.724	0.577	0.105	0.848	0.218	0.104
Data10	F	26	0.870	0.024	0.211	0.677	0.772	0.093	0.895	0.117	0.096
Mean	—	26.2	0.762	0.411	0.170	0.696	0.619	0.140	0.822	0.249	0.127

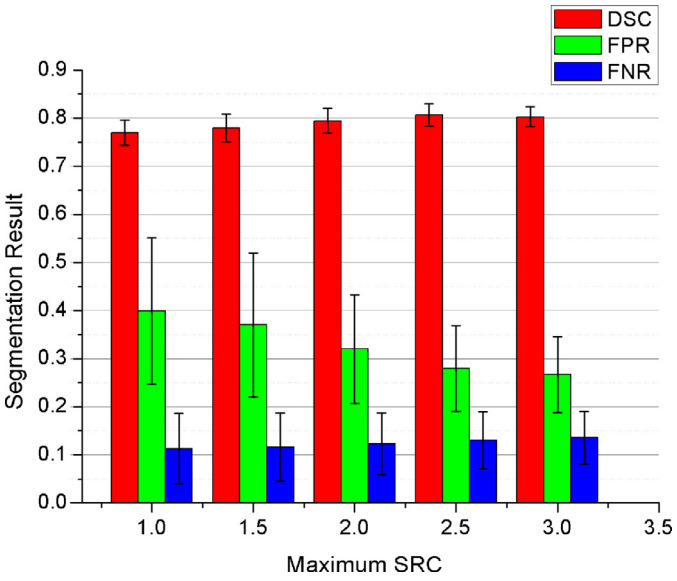

Fig. 8. Relationship between DSC, FPR, and FNR and the changes in maximum segmentation ratio coefficient (SRC).

SRC is another important parameter that should be determined. In this paper, the value of SRC in each slice is linearly interpolated by the top T_{top}=1 and bottom of head T_{bottom}=T_{max}; thus, the maximum value of SRC should only be determined. In this paper, five datasets are trained to obtain the optimal SRC for the proposed algorithm, and training results is provided for segmentation of another five datasets. Fig. 8 shows the training results that the relationship between mean and standard deviations of DSC, FPR, FNR, and the changes in the maximum SRC. The maximum SRC is sampled in [1,3] with the sampling interval of 0.5. When the maximum SRC increases from 1 to 2.5, the average value of DSC of the proposed algorithm increases from 0.770 to 0.806; when the maximum SRC increases from 2.5 to 3, the it decreases to 0.802; when the maximum SRC increases from 1 to 3, the average value of FPR decreases from 0.399 to 0.167, and the average value of FNR increases from 0.113 to 0.135. Therefore, with the increase in the maximum SRC, more noise is smoothed out and over-segmentation can be reduced, improving the accuracy of segmentation. However, this improvement will filter out some actual small blood vessels, leading to increasing under-segmentation. Besides, with the increasing of the maximum SRC from 1 to 2.5, the standard deviations of DSC, FPR and FNR immediately decrease from 0.026, 0.152 and 0.073 to 0.022, 0.089 and 0.059, respectively. With the increasing of the maximum SRC from 2.5 to 3, they slowly decrease to 0.020, 0.079 and 0.054, respectively. Therefore, 2.5 should be the optimal maximum SRC for the proposed algorithm.

Table 1 lists the segmentation results of the grayscale-based method, shape-based method, and proposed method for the 10 head PC-MRA datasets. When the grayscale-based method is applied, the average DSC, FPR, and FNR are 0.762, 0.411, and 0.170, respectively. When the shape-based method is applied, the average DSC, FPR, and FNR are 0.696, 0.619, and 0.140, respectively. When the proposed method is applied, the average DSC, FPR, and FNR are 0.822, 0.249, and 0.127, respectively. Therefore, the DSC, FPR, and FNR of the proposed method are the most satisfactory among these three compared methods. Compared with the grayscale- and shape-based methods, the DSC of the proposed method increases by 7.9% and 18.1%, respectively; correspondingly, the FPR decreases by 38.4% and 59.8%, and FNR increases by 25.3% and 9.3%.

Additionally, when the grayscale- and shape-based methods are applied, some large errors exist in some datasets. For example, when Data 5 and 7 are tested by the grayscale-based method, the corresponding FPRs are 1.290 and 1.610, respectively, which are far higher than the average. Fig. 9A1 and B1 provide the segmentation results of this method. A large amount of noise is present, which is similar to blood vessel, so segmentation through a single grayscale feature cannot remove noise. Our method of combining the vascular grayscale and shape features will overcome this difficulty (Fig. 9A2 and B2). When testing Data 6 with the shape-based method, the FPR reaches 0.926, which is far higher than the average. Fig. 9C1 presents the corresponding segmentation result. When the shape-based method is applied, large blood vessels are severely over-segmented, and the vascular structures are severely deformed. Fig. 9C2 shows that the original vascular shape can be maintained through our proposed method.

4. Discussions

Currently, combination of multi-feature is a common solution of vascular segmentation [34,35]. In this paper, an automatic vascular segmentation method combined vascular grayscale and shape features is proposed to extract accurate vascular structures from the head PC-MRA. The main advantage of the method is that it can overcome the unavoidable drawback of the extraction algorithm that based on one vascular feature. For example, only according to the grayscale feature of blood vessels, it will lose small blood vessels of weak grayscale; And depending on the vascular shape feature, non-tubular vascular structures such as abnormal blood vessel or bifurcations would be lost for these algorithms. Moreover, for presently widely used shape based multi-scale tubular segmentation method, segmented vascular structures would be inevitably become thicker. It is difficult to be solved only depending on a single feature.

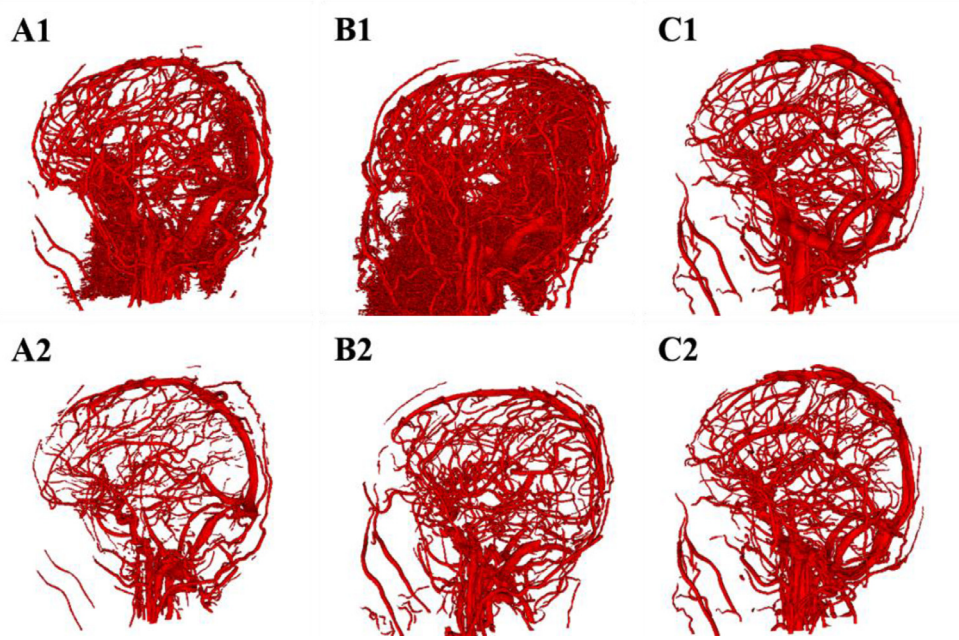

Fig. 9. Extreme segmentation results. (A1) and (B1) are the segmentation results of the grayscale-based method for Data 6 and 8, respectively; (C1) is the segmentation result of the shape-based method for Data 7; and (A2), (B2), and (C2) are the corresponding segmentation results of the proposed method.

In this paper, a series of experiments are designed to evaluate the feasibility and effectiveness of the proposed algorithm. As can be seen from Fig. 5, the vascular structures segmented based on the proposed method are most close to the manual segmentation, and it's also the most completed. Besides, some tiny blood vessels which are hardly recognized and can't be manually segmented, are identified by our proposed method. In Fig. 6, original dataset and 3D segmented vascular structures are projected onto the two-dimensional image by MIP, respectively. And it can more realistically reflect the relationship between the segmented vessels and the gold standard. It can be found that the segmented vascular structures of the proposed algorithm and the gold standard are basically the same. In order to assess the segmentation accuracy, we use DSC, FPR and FNR three indicators to represent the measurement of the segmentation, over-segmentation, and under-segmentation ratios. And these indicators are also used to confirm the selection of parameters of the proposed algorithm, such as the penalty coefficient and maximum SRC mentioned in this paper. 10 groups of clinical dataset are tested, and the average DSC, FPR and FNR of the proposed algorithm are 0.822, 0.249 and 0.127, respectively. They are all better than the other two compared algorithms. In Fig. 9, three segmentation results of large errors by traditional algorithms are given, and compared segmented structures of the proposed algorithm show that, we can still accurately extract vascular structures from bad dataset. Therefore, the proposed automatic vascular segmentation method is higher in accuracy and more stable.

5. Conclusions

Accurate 3D vascular structure segmentation from the head PC-MRA dataset is important for the planning and navigation of neurosurgery. For the traditional Bayesian vascular segmentation method based on grayscale feature, segmentation relies on the grayscale distribution of blood vessels, and small vessels might be lost because of their weak intensity information. Moreover, if a large amount of noise is present, similar to that in vessels in grayscale, over-segmentation will occur. For the multiscale vascular segmentation method based on shape feature, the multiscale space is constructed through convolution with different Gaussian functions, resulting in the thickening and deformation of vascular segmentation.

In this paper, we propose an automatic vascular segmentation method by combining the vascular grayscale and shape features to extract accurate vascular structures from the head PC-MRA dataset. First, an improved Bayesian vascular segmentation method is proposed. This method introduces a cost function in the process of statistical modeling to differentially punish the mis-segmentation of the background and blood vessels, which ensures that the vessels are obtained under an appropriate tolerance of noise. Subsequently, according to the vascular shape feature, a multiscale vascular enhancement filter is used to obtain the enhanced vesselness image, which highlights the information of blood vessels and suppresses the non-tubular structures in the background. On this basis, a vascular reconstruction image is constructed by the grayscale and shape features according to the Dempster–Shafer evidence theory, and the corresponding vascular structures are segmented by the Otsu algorithm. To remove the noise in the segmentation result, we design a vascular denoising method based on the proposed SRC according to the noise distribution in the PC-MRA dataset. This method uses the obtained vascular structures and initial segmentation result to overcome over-segmentation. To evaluate the proposed algorithm, we validate it through qualitative and quantitative analyses. From the visualization of the MC and MIP results, the segmentation results of our proposed method are observed to be closer to the actual data than that of the grayscale- and shape-based methods. Upon testing the 10 groups of clinical datasets, the proposed method is proven to be better than traditional methods in terms of segmentation accuracy, over-segmentation ratio, and under-segmentation ratio. Therefore, the proposed grayscale and shape feature-based vascular segmentation is not only effective but also accurate.

Acknowledgments

This work was supported in part by grants from National Basic Research and Key Technologies R&D Program of China

(2012BAI16B03), and the National Natural Science Foundation of China (81271671, 61361160417).

Supplementary materials

Supplementary material associated with this article can be found, in the online version, at doi:10.1016/j.cmpb.2017.02.008.

References

[1] Y. Sun, D.L. Parker, Performance analysis of maximum intensity projection algorithm for display of MRA images, IEEE Trans. Med. Imaging 18 (12) (1999) 1154–1169.
[2] L. Marquardt, W. Kuker, A. Chandratheva, O. Geraghty, P. Rothwell, Incidence and prognosis of ≥ 50% symptomatic vertebral or basilar artery stenosis: prospective population-based study, Brain. 132 (4) (2009) 982–988.
[3] M.W. Law, A.C. Chung, Segmentation of intracranial vessels and aneurysms in phase contrast magnetic resonance angiography using multirange filters and local variances, IEEE Trans. Image Process. 22 (3) (2013) 845–859.
[4] M. Kersten-Oertel, I. Gerard, S. Drouin, K. Mok, D. Sirhan, D.S. Sinclair, D.L. Collins, Augmented reality in neurovascular surgery: feasibility and first uses in the operating room, Int. J. Comput. Assist. Radiol. Surg. (2015) 1–14.
[5] G. Zombori, R. Rodionov, M. Nowell, M. Zuluaga, M.J. Clarkson, C. Micallef, B. Diehl, T. Wehner, A. Miserochi, A.W. McEvoy, A computer assisted planning system for the placement of sEEG electrodes in the treatment of epilepsy, in: Information Processing in Computer-Assisted Interventions, Springer, 2014, pp. 118–127.
[6] C. Essert, S. Fernandez-Vidal, A. Capobianco, C. Haegelen, C. Karachi, E. Bardinet, M. Marchal, P. Jannin, Statistical study of parameters for deep brain stimulation automatic preoperative planning of electrodes trajectories, Int. J. Comput. Assist. Radiol. Surg. 10 (12) (2015) 1973–1983.
[7] D. Lesage, E.D. Angelini, I. Bloch, G. Funka-Lea, A review of 3D vessel lumen segmentation techniques: Models, features and extraction schemes, Med. Image Anal. 13 (2009) 819–845.
[8] L. Wen, X. Wang, Z. Wu, M. Zhou, J.S. Jin, A novel statistical cerebrovascular segmentation algorithm with particle swarm optimization, Neurocomputing 148 (2015) 569–577.
[9] M.S. Hassouna, A.A. Farag, S. Hushek, T. Moriarty, Cerebrovascular segmentation from TOF using stochastic models, Med. Image Anal. 10 (1) (2006) 2–18.
[10] A.C. Chung, J.A. Noble, P. Summers, Vascular segmentation of phase contrast magnetic resonance angiograms based on statistical mixture modeling and local phase coherence, IEEE Trans. Med. Imaging 23 (12) (2004) 1490–1507.
[11] D.-Y. Kim, 3D volume extraction of cerebrovascular structure on brain magnetic resonance angiography data sets, J. Biomed. Sci. Eng. 5 (2012) 574–579.
[12] Y. Masutani, T. Schiemann, K.-H. Höhne, Vascular shape segmentation and structure extraction using a shape-based region-growing model, in: Medical Image Computing and Computer-Assisted Interventation—MICCAI'98, Springer, 1998, pp. 1242–1249.
[13] Y. Tian, Q. Chen, W. Wang, Y. Peng, Q. Wang, F. Duan, Z. Wu, M. Zhou, A Vessel Active Contour Model for Vascular Segmentation, BioMed Res. Int. 2014 (2014).
[14] N.D. Forkert, A. Schmidt-Richberg, J. Fiehler, T. Illies, D. Möller, D. Säring, H. Handels, J. Ehrhardt, 3D cerebrovascular segmentation combining fuzzy vessel enhancement and level-sets with anisotropic energy weights, Magn. Reson. Imag. 31 (2) (2013) 262–271.
[15] D.L. Wilson, J.A. Noble, An adaptive segmentation algorithm for time-of-flight MRA data, IEEE Trans. Med. Imaging 18 (10) (1999) 938–945.
[16] G. Agam, C. Wu, Probabilistic modeling based vessel enhancement in thoracic CT scans, in: Computer Vision and Pattern Recognition, 2005. CVPR 2005. IEEE Computer Society Conference on, IEEE, 2005, pp. 649–654.
[17] A.C. Chung, J.A. Noble, Statistical 3D vessel segmentation using a Rician distribution, in: Medical Image Computing and Computer-Assisted Intervention–MICCAI'99, Springer, 1999, pp. 82–89.
[18] F.K. Quek, C. Kirbas, Vessel extraction in medical images by wave-propagation and traceback, IEEE Trans. Med. Imaging 20 (2) (2001) 117–131.
[19] R. Wang, C. Li, J. Wang, X. Wei, Y. Li, Y. Zhu, S. Zhang, Threshold segmentation algorithm for automatic extraction of cerebral vessels from brain magnetic resonance angiography images, J. Neurosci. Methods 241 (2015) 30–36.
[20] A. Chung, J.A. Noble, P. Summers, Fusing speed and phase information for vascular segmentation of phase contrast MR angiograms, Med. Image Anal. 6 (2) (2002) 109–128.
[21] O. Friman, M. Hindennach, C. Kühnel, H.O. Peitgen, Multiple hypothesis template tracking of small 3D vessel structures, Med. Image Anal. 14 (2) (2010) 160–171.
[22] Z. Shoujun, Y. Jian, W. Yongtian, C. Wufan, Automatic segmentation of coronary angiograms based on fuzzy inferring and probabilistic tracking, BioMed. Eng. OnLine 9 (2010) 1–21.
[23] C. Lorenz, I.C. Carlsen, T. Buzug, C. Fassnacht, J. Weese, Multi-scale line segmentation with automatic estimation of width, contrast and tangential direction in 2D and 3D medical images, in: CVRMed-MRCAS'97, Springer, 1997, pp. 233–242.
[24] Y. Sato, S. Nakajima, N. Shiraga, H. Atsumi, S. Yoshida, T. Koller, G. Gerig, R. Kikinis, Three-dimensional multi-scale line filter for segmentation and visualization of curvilinear structures in medical images, Med. Image Anal. 2 (2) (1998) 143–168.
[25] A. Frangi, W. Niessen, K. Vincken, M. Viergever, Multiscale vessel enhancement filtering, in: Medical Image Computing and Computer-Assisted Intervention—MICCAI'98, 1998, pp. 130–137.
[26] X. Du, H. Ding, W. Zhou, G. Zhang, G. Wang, Cerebrovascular segmentation and planning of depth electrode insertion for epilepsy surgery, Int. J. Comput. Assist. Radiol. Surg. 8 (6) (2013) 905–916.
[27] R. Xiao, J. Yang, D. Ai, J. Fan, Y. Liu, G. Wang, Y. Wang, Adaptive ridge point refinement for seeds detection in X-ray coronary angiogram, Comput. Math. Methods Med. (2015).
[28] D.P. Zhang, Coronary Artery Segmentation and Motion Modelling, Imperial College, London, 2010.
[29] T. Lindeberg, Scale-Space Theory in Computer Vision, Springer, 1994.
[30] T. Lindeberg, Edge detection and ridge detection with automatic scale selection, Int. J. Comput. Vision 30 (2) (1998) 117–154.
[31] N. Otsu, A threshold selection method from gray-level histograms, Automatica 11 (1975) 23–27.
[32] O. Basir, X. Yuan, Engine fault diagnosis based on multi-sensor information fusion using Dempster–Shafer evidence theory, Inf. Fusion 8 (4) (2007) 379–386.
[33] D. Rajon, W. Bolch, Marching cube algorithm: review and trilinear interpolation adaptation for image-based dosimetric models, Comput. Med. Imaging. Graph. 27 (5) (2003) 411–435.
[34] S. Aslani, H. Sarnel, A new supervised retinal vessel segmentation method based on robust hybrid features, Biomed. Signal Process. Control 30 (2016) 1–12.
[35] Y.Z. Zeng, Y.Q. Zhao, M. Liao, B.J. Zou, X.F. Wang, W. Wang, Liver vessel segmentation based on extreme learning machine, Physica Med. 32 (2016) 709–716.